RSC Advances

ROYAL SOCIETY OF CHEMISTRY

PAPER

View Article Online
View Journal | View Issue

Check for updates

Cite this: *RSC Adv.*, 2020, **10**, 12373

Poly(fluorenone-*co*-thiophene)-based nanoparticles for two-photon fluorescence imaging in living cells and tissues†

Nan Du,[ab] Ying Tan,[ab] Chen Zhang[ab] and Chunyan Tan*[ab]

Received 21st February 2020
Accepted 19th March 2020

DOI: 10.1039/d0ra01664k

rsc.li/rsc-advances

Conjugate polymer nanoparticles (CPNs) were constructed based on poly(fluorenone-*co*-thiophenes) (PFOTs) synthesized through a direct arylation polymerization (DArP) approach. Results demonstrate that the developed novel CPNs have potential applications in two-photon fluorescence imaging of both cells and tissues.

Fluorescence imaging has been widely applied in biological studies on subcellular microenvironments and tissues to develop disease diagnostic methods and clinical treatment.[1–3] The emerging two-photon fluorescence imaging approach has demonstrated some advantages over traditional single-photon fluorescence imaging, including deeper penetration depth, less photo-damage, reduced self-absorption and background signal due to autofluorescence, *etc.*[4–6] Several two-photon absorption (TPA) materials have been reported thus far, such as organic molecules, quantum dots, metal complexes, carbon quantum dots, graphene quantum dots, *et al.*,[7–11] both small-molecule fluorescent probes and nano-sized imaging agents fabricated by CPs are attractive and versatile materials for studying biological systems, and their size, composition, surface ligands, optical properties are important for their application.[12–14] So, developing new TPA materials remains challenging but is needed to improve fluorescence quantum yield, biocompatibility, photostability, and ease of preparation compared to existing TPA probes.

Conjugated polymers (CPs) with extended π-conjugation structure have been studied as promising fluorescent probes over the past two decades. Due to their effective absorption and fluorescence, high photostability, signal amplification effect, and excellent biocompatibility, they have been widely implemented in biosensing, drug delivery, and imaging.[15–19] For instance, CPs-based nanoparticles with two-photon excitation character were applied as high contrast cell imaging probes by Xu *et al.*[20,21] It was reported that synthesized chromophores with donor–acceptor (D–A) structures, which tend to exhibit relatively large two-photon absorption cross-section, and thus, enhanced TPA properties by the charge transfer effect.[22,23] Wu *et al.* fabricated CPNs with polyfluorene derivative that were characterized by cross sections values up to 2.0 × 10^5 GM.[24] Recently, Schanze *et al.* reported anionic conjugated polyelectrolytes (CPEs), such as PPE-SO_3^-, with moderate two-photon absorption cross-sections in the near-infrared (NIR) region for two-photon fluorescence cell imaging.[25] Their work disclosed the potentials of CPEs and CPNs as TPA fluorescent materials in tissue imaging.

Herein, we developed novel PFOT-based nanoparticles to exploit their single- and two-photon fluorescence properties for imaging applications in living cells and tissues (Scheme 1).

Direct arylation polymerization (DArP) has emerged as a simple and atom-economic method for polymer synthesis compared to traditional metal-catalyzed coupling polymerization, as shown in Fig. 1a.[26] In this work, 4 novel D–A type CPs composed of fluorenone and thiophene moieties were synthesized *via* the DArP method, as displayed in Fig. 1b and c. All

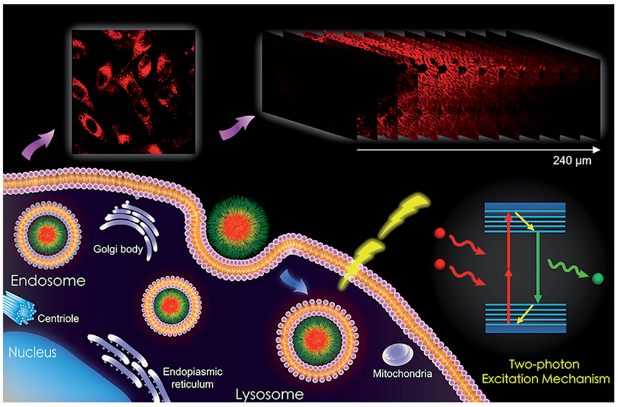

Scheme 1 Illustration of PFOT nanoparticles as two-photon imaging probes.

---

[a] *Department of Chemistry, Tsinghua University, Beijing, 100084, P. R. China*

[b] *State Key Laboratory of Chemical Oncogenomic, Tsinghua Shenzhen International Graduate School, Tsinghua University, Shenzhen, 518055, P. R. China. E-mail: tancy@sz.tsinghua.edu.cn; Fax: +86-755-26032094; Tel: +86-755-26036533*

† Electronic supplementary information (ESI) available: Experimental including materials, general methods, synthesis, some supplementary spectra and tables. See DOI: 10.1039/d0ra01664k

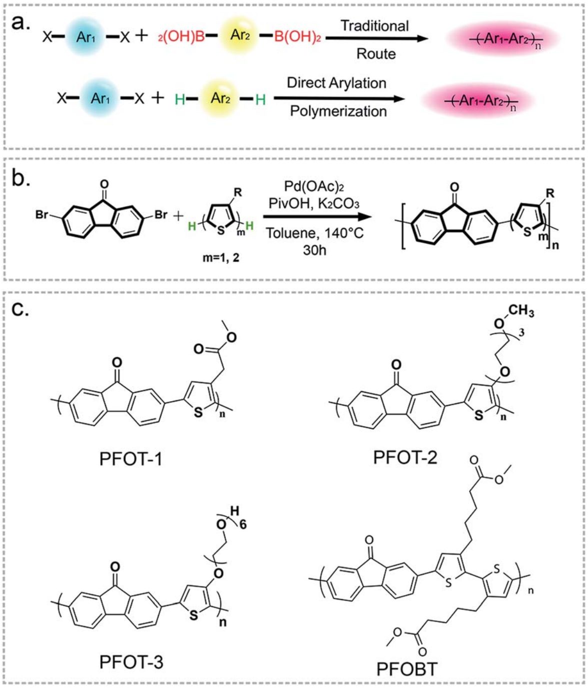

Fig. 1 (a) Comparison of traditional coupling reactions and direct arylation polymerization, X is halogen. (b) Designed synthetic route of novel poly(fluorenone-*co*-thiophene) conjugated polymer. (c) Acquired novel poly(fluorenone-*co*-thiophene) (PFOT) conjugated polymers.

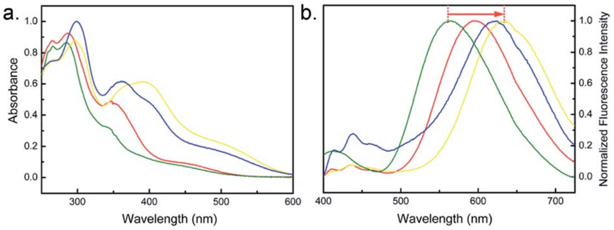

Fig. 2 Absorption (a) and fluorescence emission spectra (b) of PFOT-1 (red), PFOT-2 (yellow), PFOT-3 (blue), and PFOBT (green) polymers in $CHCl_3$, $\lambda_{ex} = 380$ nm. The concentration of all polymers is 10 μM in chloroform.

polymers are soluble in typical organic solvents, such as chloroform, THF, methanol, acetone, and DMF. PFOT-2 and PFOT-3 are slightly soluble in water due to the increased length of their hydrophilic side chains. Under optimized experimental conditions, we acquired PFOT-1, PFOT-2, PFOT-3, and PFOBT with reasonable Mn of 1.99, 2.57, 5.14, and 4.76 kg mol^{-1} respectively.

Photophysical properties of CPs are affected by their main chain conjugated structure, molecular weight, side chain structure, solvent, and *etc.* For the fluorenone-based copolymers, it has been reported that the intermolecular CO⋯HC (aromatic) hydrogen bonds (H-bonds) would exert influence on absorption maximum position.[27,28] In addition, side chains of the CPs could also have impact on the conformation of the backbone and the aggregation state of the polymers. Photophysical properties of the obtained four CPs (PFOT-1, PFOT-2, PFOT-3, and PFOBT) were studied. UV-visible absorption and fluorescence emission spectra of the four CPs in chloroform are shown in Fig. 2a. The absorption of all the four polymers in chloroform features a strong band in the UV range and a broader and weaker band in the visible range. PFOT-1 and PFOBT show UV absorption with two maxima at 287 and 265 nm, that are assigned, respectively, to cisoid and transoid conformations of the conjugated backbone, while PFOT-2 and PFOT-3 only demonstrate one peak at about 305 nm, suggesting that the cisoid conformation dominates which enhance the polymer aggregation. Strong and wide fluorescence emission bands of the 4 polymers can be observed with the full width at half maxima (FWHM) at about 200 nm (Fig. 2b). Polymers with single thiophene in their repeat units, such as PFOT-1, PFOT-2, and PFOT-3, demonstrated red-shifted emission maximum wavelengths (595 to 630 nm) compared to that of the polymer PFOBT (555 nm), which contains bithiophene in its repeat units. We believe that PFOBT is in a less aggregated state than all other three PFOT polymers, leading to a blue-shifted absorption and emission band. It has been reported that D–A type CPs usually demonstrate lower bandgaps and large Stokes shifts due to the intramolecular charge transfer (ICT).[29] As the spectra shown, PFOT-1, PFOT-2, PFOT-3, and PFOBT CPs exhibit large Stokes shifts of 220, 260, 250, and 170 nm respectively, which is in favour of diminishing the reabsorption effect. Quantum yields (QYs) of PFOT-1, PFOT-2, PFOT-3, and PFOBT CPs in $CHCl_3$ were determined to be 0.081, 0.193, 0.376, and 0.432, respectively, *via* the reference method with coumarin 6 in ethanol as a reference. Then, PFOT-2, PFOT-3, and PFOBT were selected for further imaging studies.

For bio-imaging, efficient internalization of probes by cells is an essential step. In order to improve the biocompatibility of the CPs, CPNs were fabricated *via* the nanoprecipitation method using polymers and Pluronic-F127 as a surfactant and encapsulation matrix, as shown in Fig. 3a. The diameters of CPNs were characterized by dynamic light scattering (DLS) for

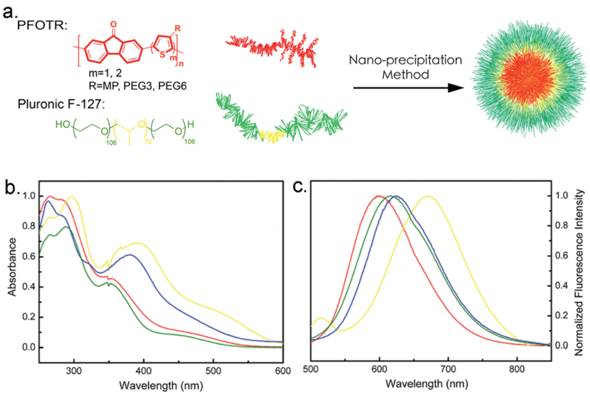

Fig. 3 (a) Fabrication of CPNs *via* nanoprecipitation method. Absorption (b) and fluorescence emission (c) spectra of PFOT-1 (red), PFOT-2 (yellow), PFOT-3 (blue), and PFOBT (green) NPs in water, $\lambda_{ex} =$ 480 nm (b).

Table 1 Characterization of PFOT series CPNs

Sample name	D^a (nm)	PDI^a	QYs^b	Stokes shift^c
PFOT-1	91.7 ± 1.5	0.12	0.012	120
PFOT-2	82.6 ± 0.5	0.17	0.021	200
PFOT-3	142.3 ± 1.9	0.44	0.029	150
PFOBT	45.1 ± 0.5	0.32	0.027	145

[a] The hydrodynamic diameter (Dh) and polydispersity index (PDI) of PFOT nanoparticles. [b] Quantum yields (QYs) were measured *via* the reference method with coumarin 6 in ethanol as a reference. [c] Stokes shift of PFOT series CPNs.

three times with the average diameters range from 45.1 to 142.3 nm (Table 1). Fig. S3† revealed the core–shell morphology of the CPNs, probably formed by the hydrophobic inner cores and hydrophilic outer shells. This core–shell morphology of the CPNs helps with improving their stability in aqueous environment, and demonstrates their potential application as fluorescent probes and drug nano-vehicles. In Fig. 3b, compared to the corresponding CPs in solutions, fluorescence emission spectra of the four CPNs revealed red-shifts. This may be ascribed to the internal stress of the particles that increases with the formation of CPNs, which leads to variation in the energy band structures, incremental overlap of the electron wave function, narrowing of energy band-gap, and red-shift of the emission peak length.[30] Also, it has been reported that aggregated particles fabricated *via* nanoprecipitation method usually exhibit red-shifted emission compared to their non-aggregated forms, which can be ascribed to the bending, kinking, and interchain interactions of polymer backbones in the aggregation.[31,32] Cellular cytotoxicity assay of the PFOT CPNs towards HeLa cells displayed no apparent cytotoxicity with a concentration up to 200 μg mL^{-1} as shown in Fig. 4a. The low cytotoxicity and efficient endocytosis (Fig. S4†) demonstrated a good biocompatibility of the synthesized CPNs. Also, the photostability assay of PFOT-2 NPs, PFOT-3 NPs, and PFOBT NPs was carried out *via* a photobleaching experiment. As shown in Fig. 4b and c, fluorescence of PFOT-2 NPs, PFOT-3 NPs, PFOBT NPs, and LysoTracker Green remained at 55%, 54%, 54%, and 8% respectively, after 20 times scans, suggesting that the CPNs exhibited stronger photostability than the small molecular probe LysoTracker Green. Our results also show that the CPs and CPNs are stable at pH ranging from 5.0–7.4, which

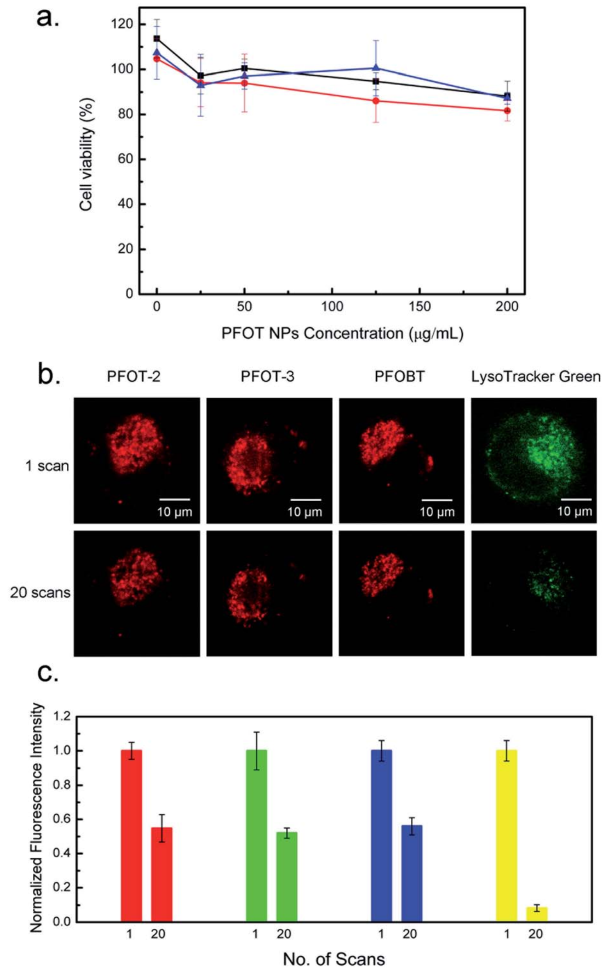

Fig. 4 (a) Cell viability of HeLa cells after treatment with PFOT-2 (black), PFOT-3 (red), and PFOBT (blue) NPs at the concentration range from 0 to 200 μg mL^{-1}. Cells without treatment of NPs were used as control. (b) Photobleaching measurements: fluorescent images of HeLa cells cultured with the CPNs and LysoTracker Green respectively at 1 scan and 20th scan. (c) The cellular fluorescence intensity of PFOT-2 (red), PFOT-3 (green), PFOBT (blue) NPs, and LysoTracker Green (yellow) respectively *vs.* the number of scans.

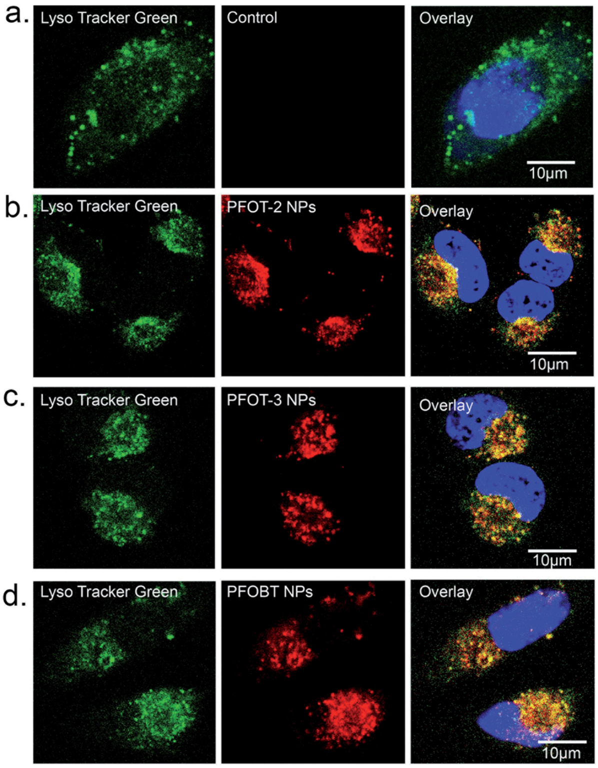

Fig. 5 Fluorescence imaging of intracellular distribution of PFOT-2 NPs (b), PFOT-3 NPs (c) and PFOBT NPs (d), respectively, co-stained with LysoTracker Green (66.7 nM) and DAPI (blue channel) in HeLa cells. Polymer concentration is 5 μM. For control group (a), cells were washed before imaging.

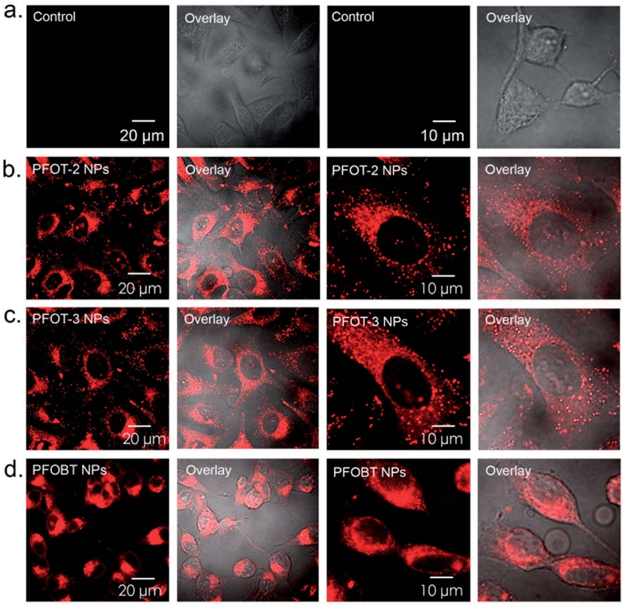

Fig. 6 Two-photon imaging of HeLa cells incubated with PFOT-2 NPs (b), PFOT-3 NPs (c), and PFOBT NPs (d), respectively (NPs at 5 μM, λ_{ex} = 720 nm, emission wavelength ranged from 575 to 645 nm). The 3rd and 4th columns are magnification of the corresponding groups. For control experiment (a), cells were washed before imaging (λ_{ex} = 960 nm).

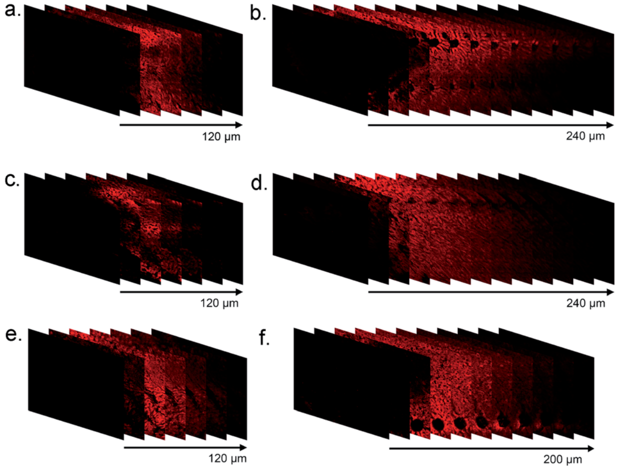

Fig. 7 Fluorescence imaging of fresh mice liver tissue slices incubated with NPs (10 μM) for 1 h in PBS buffer at different penetration depths. PFOT-2 NPs (a and b), PFOT-3 NPs (c and d), and PFOBT (e and f) NPs tissue imaging of one-photon (left) ($\lambda_{ex} = 559$ nm, $\lambda_{em} = 575–675$ nm) and two-photon condition (right) ($\lambda_{ex} = 960$ nm for PFOT-2 NPs, PFOT-3 NPs, $\lambda_{ex} = 720$ nm for PFOBT NPs, $\lambda_{em} = 575–645$ nm). The step size is 20 μm.

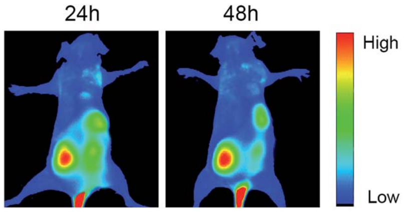

Fig. 8 *In vivo* fluorescence images of 4T1 tumor (on the lower left side of the mouse's back) bearing BALB/c mouse injected with PFOBT NPs at 24 h and 48 h post-injection. ($\lambda_{ex} = 470$ nm, $\lambda_{em} = 600$ nm).

cover the biological pH ranges of tumor tissues, late endosomes and lysosomes, normal tissues and blood (Fig. S6†).

Then, HeLa cells were incubated with PFOT-2, PFOT-3, and PFOBT NPs (concentration of 5 μM each) for 4 h and observed with a one-photon confocal fluorescence microscope. As shown in Fig. S4,† almost all cells demonstrated CPNs internalization signals of red fluorescence. Furthermore, to explore the endocytosis process of these CPNs, organelle location was investigated *via* a lysosome co-localization probe, LysoTracker green. Fig. 5 displays the fluorescence imaging of HeLa cells co-stained with CPNs (red) and the LysoTracker probe (green). As shown in Fig. 5, red signal of PFOT-2, PFOT-3, and PFOBT NPs and green signal well overlapped with Pearson correlation coefficients (PCCs) of 0.94 (±0.03), 0.94 (±0.02), and 0.97 (±0.02), respectively. This means that most NPs localized in lysosomes, while others appear in early or late endosomes, suggesting that lysosomes are the primary organelle participating in the endocytosis process of these CPNs.[33]

Many researchers have high interest in investigating D–A type CPs with TPA property for use in photoelectric devices and bio-probes.[34,35] It has been acknowledged that molecules constructed by electron donating and accepting functional groups with extended π-conjugated systems are capable of displaying two-photon absorption cross-sections.[36,37] In this work, the application of PFOT CPNs as two-photon imaging probes were explored by an Olympus FVMPE RS two-photon microscope with femtosecond laser excitation at 720 and 960 nm. The pictures taken by the two-photon microscope in Fig. 6 show that 5 μM of CPNs is sufficient to give clear cells fluorescent images of high quality with an emission wavelength range of 575–645 nm. It should also be noted that both excitation and emission wavelengths of CPNs are located in the 575–960 nm range, encompassing the deep red and near-infrared areas. Combining these properties, PFOT CPNs as NIR probes could provide both deep tissue penetration and low autofluorescence, which has great potential in medical fluorescent imaging applications. To further verify the advantages of deep-red emission and two-photon absorption of PFOT CPNs, fluorescence images of mice liver tissue slices were studied. The tissue slices were pre-treated with PFOT-2, PFOT- 3, and PFOBT NPs for 1 h, then one-photon and two-photon confocal imaging in Z-scan mode were performed to obtain fluorescence images as shown in Fig. 7. All the PFOT CPNs were effectively applied as tissue imaging probes with penetration depths of 120–240 μm. Compared with one-photon confocal Z-scan imaging, two-photon Z-scan imaging showed a deeper penetration depth up to 240 μm due to the longer absorption and emission wavelength in deep red and NIR areas. All results suggest that the CPNs based on PFOT polymers possess excellent tissue-penetrating, staining, and imaging capabilities. Also, to investigated the *in vivo* NIR fluorescence imaging ability of PFOBT

NPs, we established the common BALB/c murine breast cancer (4T1) model. As shown in Fig. 8, the PFOBT CPNs were able to accumulate in tumor tissue efficiently after 48 h tail vein injection, due to the enhanced permeability and retention (EPR) effect.

Conclusions

In summary, we designed and synthesized a series of new CPs with poly(fluorenone-*co*-thiophene) backbones *via* DArP. The PFOT series CPs exhibit long emission wavelength ranges of 500–800 nm and two-photon absorption property, which allows for longer excitation wavelengths of 720 and 960 nm located in the deep red and NIR areas. CPNs based on PFOT polymers also demonstrated good biocompatibility, high photostability, excellent lysosome co-localization, and two-photon imaging properties, with a much deeper tissue penetration than one-photon confocal imaging. In this work, the novel PFOT CPNs provide new insight and perspectives for fabricating TPA NPs with novel backbones and demonstrate their application potentials in NIR *in vitro* and *in vivo* imaging.

Conflicts of interest

There are no conflicts to declare.

Acknowledgements

The authors would like to acknowledge the financial support from the National Natural Science Foundation of China (NSFC No. 21572115), and the Shenzhen Bay Laboratory Open Funding (SZBL2019062801009).

Notes and references

1 K. P. Carter, A. M. Young and A. E. Palmer, *Chem. Rev.*, 2014, **114**, 4564–4601.
2 H. Peng and D. T. Chiu, *Chem. Soc. Rev.*, 2015, **44**, 4699–4722.
3 W. K David and H. Niko, *Chem. Soc. Rev.*, 2015, **44**, 4792–4834.
4 Y. Shen, A. J. Shuhendler, D. Ye, J. J. Xu and H. Y. Chen, *Chem. Soc. Rev.*, 2016, **45**, 6725–6741.
5 Y. Sheng and K. D. Belfield, *Eur. J. Org. Chem.*, 2012, **17**, 3199–3217.
6 F. Helmchen and W. Denk, *Nat. Methods*, 2005, **2**, 932–940.
7 B. Swagata, E. B. Veale, C. M. Phelan, S. A. Murphy, G. M. Tocci, L. J. Gillespie, D. O. Frimannsson, J. M. Kelly and G. Thorfinnur, *Chem. Soc. Rev.*, 2014, **44**, 1601–1618.
8 H.-W. Liu, L. Chen, C. Xu, Z. Li, H. Zhang, X.-B. Zhang and W. Tan, *Chem. Soc. Rev.*, 2018, **47**, 7140–7180.
9 D. Wu, A. C. Sedgwick, T. Gunnlaugsson, E. U. Akkaya, J. Yoon and T. D. James, *Chem. Soc. Rev.*, 2017, **46**, 7105–7123.
10 Y. Shen, A. J. Shuhendler, D. Ye, J.-J. Xu and H.-Y. Chen, *Chem. Soc. Rev.*, 2016, **45**, 6725–6741.
11 J. Sun, Q. Xin, Y. Yang, H. Shah, H. Cao, Y. Qi, J. R. Gong and J. Li, *Chem. Commun.*, 2018, **54**, 715–718.
12 H. M. Kim and B. R. Cho, *Chem. Rev.*, 2015, **115**, 5014–5055.
13 M. Pawlicki, H. Collins, R. Denning and H. Anderson, *Angew. Chem., Int. Ed.*, 2009, **48**, 3244–3266.
14 J. Olesiak-Banska, M. Waszkielewicz, P. Obstarczyk and M. Samoc, *Chem. Soc. Rev.*, 2019, **48**, 4087–4117.
15 J. Hui, T. Prasad, J. R. Reynolds and K. S. Schanze, *Angew. Chem.*, 2009, **48**, 4300–4316.
16 F. Liheng, Z. Chunlei, Y. Huanxiang, L. Libing, L. Fengting and W. Shu, *Cheminform*, 2014, **44**, 6620–6633.
17 J. Yu, Y. Rong, C. T. Kuo, X. H. Zhou and D. T. Chiu, *Anal. Chem.*, 2017, **89**, 42–56.
18 X. Xinjun, L. Ronghua and L. Lidong, *Chem. Commun.*, 2015, **51**, 16733–16749.
19 P. Johannes and M. Stefan, *Chem. Rev.*, 2010, **110**, 6260–6279.
20 L. Shuang, S. Xiaoqin, L. Lin, Y. Peiyan, G. Zhenping, S. Q. Yao and X. Qing-Hua, *Langmuir*, 2014, **30**, 7623–7627.
21 S. Xiaoqin, L. Lin, W. Hao, S. Q. Yao and X. Qing-Hua, *Nanoscale*, 2011, **3**, 5140–5146.
22 M. Rumi, J. E. Ehrlich, A. A. Heikal, J. W. Perry, S. Barlow, Z. Hu, D. McCord-Maughon, T. C. Parker, H. Röckel and S. Thayumanavan, *J. Am. Chem. Soc.*, 2000, **122**, 9500–9510.
23 M. Albota, D. Beljonne, J. L. Brédas, J. E. Ehrlich, J. Y. Fu, A. A. Heikal, S. E. Hess, T. Kogej, M. D. Levin and S. R. Marder, *Science*, 1998, **281**, 1653–1656.
24 C. Wu, C. Szymanski, Z. Cain and J. McNeill, *J. Am. Chem. Soc.*, 2007, **129**, 12904–12905.
25 A. Parthasarathy, H. Y. Ahn, K. D. Belfield and K. S. Schanze, *ACS Appl. Mater. Interfaces*, 2010, **2**, 2744–2748.
26 X. Pang, Y. Tan, C. Tan, W. Li, N. Du, Y. Lu and Y. Jiang, *ACS Appl. Mater. Interfaces*, 2019, **11**, 28246–28253.
27 N. A. Kukhta, D. A. da Silva Filho, D. Volyniuk, J. V. Grazulevicius and G. Sini, *Chem. Mater.*, 2017, **29**, 1695–1707.
28 A. Saeki, T. Fukumatsu and S. Seki, *Macromolecules*, 2011, **44**, 3416–3424.
29 B. Jana, A. Ghosh and A. Patra, *J. Phys. Chem. Lett.*, 2017, **8**, 4608–4620.
30 B. Muthuraj, S. Mukherjee, C. R. Patra and P. K. Iyer, *ACS Appl. Mater. Interfaces*, 2016, **8**, 32220–32229.
31 Y. H. Chan and P.-J. Wu, *Part. Part. Syst. Charact.*, 2015, **32**, 11–28.
32 N. Feiner-Gracia, M. Buzhor, E. Fuentes, S. Pujals, R. J. Amir and L. Albertazzi, *J. Am. Chem. Soc.*, 2017, **139**, 16677–16687.
33 L. Zhou, F. Lv, L. Liu and S. Wang, *ACS Appl. Mater. Interfaces*, 2017, **9**, 27427–27432.
34 S. Wang, Z. Li, X. Liu, S. Phan, F. Lv, K. D. Belfield, S. Wang and K. S. Schanze, *Chem. Mater.*, 2017, **29**, 3295–3303.
35 W. Zhang, J. Kang, P. Li, L. Liu, H. Wang and B. Tang, *Chem. Commun.*, 2016, **52**, 13991–13994.
36 X. Shen, L. Li, H. Wu, S. Q. Yao and Q. H. Xu, *Nanoscale*, 2011, **3**, 5140–5146.
37 M. Pawlicki, H. A. Collins, R. G. Denning and H. L. Anderson, *Angew. Chem., Int. Ed.*, 2010, **48**, 3244–3266.